Journal of Catalysis **182,** 13–29 (1999)
Article ID jcat.1998.2306, available online at http://www.idealibrary.com on IDEAL®

NaY Zeolite-Supported Rhodium and Iridium Cluster Catalysts: Characterization by X-ray Absorption Spectroscopy during Propene Hydrogenation Catalysis

W. A. Weber, A. Zhao, and B. C. Gates[1]

Department of Chemical Engineering and Materials Science, University of California, Davis, California 95616

Received March 20, 1998; revised October 5, 1998; accepted October 12, 1998

Clusters of rhodium and of iridium were synthesized in the cages of the sodium form of the faujasite zeolite Y by decarbonylation of zeolite-supported $[Rh_6(CO)_{16}]$ or $[Ir_4(CO)_{12}]$ in H_2 at 200 or 300°C, respectively. Larger clusters (aggregates) of rhodium or iridium consisting of 10 to 20 atoms each on average were formed by treatment of zeolite-supported $[Rh_6(CO)_{16}]$ or $[Ir_6(CO)_{16}]$ in H_2 at 250 or 300°C. The samples were characterized by extended X-ray absorption fine structure (EXAFS) spectroscopy under vacuum and in (a) H_2, (b) propene, and (c) H_2/propene mixtures (with catalytic hydrogenation taking place). The EXAFS data indicate that the clusters or aggregates were intact, with the metal frames changed undetectably in the presence of any of the gases, even during catalysis and at temperatures up to 140°C. In the presence of propene only, rhodium clusters showed changes in their X-ray absorption near-edge spectra, but the iridium clusters did not. When propene was present with H_2 during catalysis, the near-edge spectra were essentially the same as those characterizing the metal clusters (or aggregates) in H_2 only. The data are consistent with the inference that the metal clusters, approximated as predominantly Ir_4 or Rh_6 (the latter not fully decarbonylated) are catalytically active themselves, as are larger aggregates of those metals.

INTRODUCTION

Many of the advances in understanding of metal catalysis have arisen from ultrahigh-vacuum surface science experiments with single metal crystals. Notwithstanding landmark advances in this understanding resulting from investigations of surface and adsorbate structures, the possibility of complications such as corrosive chemisorption casts doubt on the extrapolation of structures determined under vacuum to those present during catalysis.

Recently, techniques such as scanning tunneling microscopy (STM) have begun to provide structures of surfaces and adsorbates during catalytic reactions, even at elevated temperatures (1–5). For example, islands of coke on Pt (111) surfaces (1), benzene on step edges of Rh (111) (2), and active sites for CO oxidation on Cu (110) surfaces (3) have been identified with STM. Infrared and Raman spectroscopies also help to determine structures of working catalysts; X-ray absorption spectroscopy has provided information about changes in supported copper particles occurring during methanol synthesis catalysis (6). The spectroscopic methods are for the most part less than sufficient for determining structures of catalytic species, however, unless these species are simple and uniform enough—i.e., nearly molecular, such as single-metal-atom titanium complexes on supports (7, 8).

Metal clusters constitute a bridge between nearly molecular species and surfaces (9, 10). Precisely synthesized supported metal clusters have been prepared by removal of ligands from organometallic precursors {e.g., $[Ir_4(CO)_{12}]$, $[Ir_6(CO)_{16}]$, $[Rh_6(CO)_{16}]$, and $[Rh_6(CO)_{15}]^{2-}$ (11–18)} and shown by extended X-ray absorption fine structure (EXAFS) spectroscopy to have almost unique and nearly molecular structures, approximated, for example, as Ir_4 and Ir_6, on MgO (11, 12), γ-Al_2O_3 (13, 14), and zeolite Y (15, 16), and clusters of rhodium approximated as Rh_6 in zeolites Y and X (17, 18). Being small and nearly uniform, these supported clusters are good candidates for structural characterization in the working state.

In the research described here, metal clusters in the pores of a faujasite (zeolite Y in the sodium form), identified as predominantly $[Rh_6(CO)_{16}]$, $[Ir_4(CO)_{12}]$, or $[Ir_6(CO)_{16}]$, were treated to remove the carbonyl ligands, and the resulting structures were characterized by EXAFS spectroscopy under vacuum and in the presence of (a) H_2, (b) propene, and (c) catalytically reacting mixtures of H_2 and propene. The results show that the decarbonylation of the precursor metal carbonyl clusters led to the formation of clusters with metal frames almost as small as those of the precursors or to larger aggregates of metal, depending on the conditions. The clusters as well as the aggregates were found to be intact in the various gas atmospheres and during catalysis; thus, the clusters themselves, as well as the aggregates, are inferred to be the catalytic species for propene hydrogenation.

[1] To whom correspondence should be addressed.

0021-9517/99 $30.00

EXPERIMENTAL METHODS

Materials

Syntheses and sample transfers were conducted with exclusion of air and moisture on a double-manifold Schlenk vacuum line and in a Vacuum Atmospheres glovebox filled with N_2 that was recirculated through traps containing particles of copper and zeolite to remove traces of O_2 and moisture; typical O_2 and water concentrations were <2 and 1 ppm, respectively. Propene, N_2, H_2, and He with purities of 99.999% and CO (Puritan Bennett, UHP grade) were also purified by passage through traps. Pentanes (Fisher, HPLC grade) were dried over sodium benzophenone ketyl and then deoxygenated by purging with flowing N_2 for 2 h. $[Rh(CO)_2(acac)]$ [dicarbonylacetylacetonato rhodium (I)] (Strem, 99%) and $[Ir(CO)_2(acac)]$ [dicarbonylacetylacetonato iridium (I)] (Strem, 99%) were used as received. Zeolite Y in the sodium form was provided by the Davison Division of W. R. Grace and Company; the Si : Al atomic ratio was 9.6.

Sample Preparation

Preparation and handling of the air-sensitive materials were carried out on a Schlenk vacuum line and in the glovebox. The zeolite sample with a low water content was prepared by flowing O_2 through the untreated powder at 300°C for 4 h. This treatment was followed by evacuation at 300°C for 12 h; the sample was then cooled under vacuum to room temperature and unloaded in the glovebox. Zeolite-supported samples containing rhodium or iridium were made by dissolving $[Rh(CO)_2(acac)]$ or $[Ir(CO)_2(acac)]$ (60 mg/g of zeolite) in dried pentanes and mixing the solution with zeolite that had either been evacuated at room temperature for 12 h or calcined. In each preparation, the support was slurried with the precursor in dried pentanes in a Schlenk flask under N_2. After stirring at room temperature for several days, the solvent was removed by evacuation and the solid dried *in vacuo* (pressure $<10^{-3}$ Torr) overnight. The resulting solids were stored in the drybox. Carbonylation of the samples formed by adsorption of either $[Rh(CO)_2(acac)]$ or $[Ir(CO)_2(acac)]$ in the zeolite was carried out in a tubular flow reactor. Typically, 3 g of sample was loaded into the reactor and treated in flowing CO for 12 h at 2 atm and a predetermined temperature to give metal carbonyl clusters ($[Ir_4(CO)_{12}]$, 40°C; $[Rh_6(CO)_{16}]$, 125°C; and $[Ir_6(CO)_{16}]$, 175°C). The powder was then unloaded in the drybox and characterized by infrared spectroscopy and EXAFS spectroscopy.

Infrared Spectroscopy

Transmission infrared spectra of the samples were collected with a Bruker IFS-66V spectrometer with a spectral resolution of 0.1 cm^{-1}. Samples of the supported precursors and samples prepared by carbonylation were pressed into thin self-supporting wafers in the drybox and loaded into a controlled-atmosphere infrared cell. The temperature-controlled cell (part of a flow system) was connected to a gas manifold allowing flow of He, H_2, and CO. Each sample was scanned 64 times and the signal averaged. The spectra of the sample were ratioed to the spectrum of air.

X-ray Absorption Spectroscopy

The X-ray absorption spectroscopy experiments were performed on X-ray beamline X-11A at the National Synchrotron Light Source (NSLS) at Brookhaven National Laboratory (Upton, NY). The storage ring operated at an energy of 2.5 GeV with ring currents of 140–240 mA. Transmission EXAFS and X-ray absorption near edge spectroscopy (XANES) experiments were carried out with wafers prepared in an N_2-filled glovebox at the synchrotron. A powder sample in the glovebox was placed in a holder in the glove box, which was then placed in a die and pressed into a self-supporting wafer. The wafer was loaded into an EXAFS cell (19) and sealed. Typically, the cell was evacuated immediately after removal from the glovebox.

X-ray absorption spectra were recorded with each reference compound (Table 1) and each catalyst sample under vacuum and at temperatures between −150 and 140°C. Furthermore, each sample was scanned in the presence of various gases and under catalytic reaction conditions; details are given in Tables 2–5. Higher harmonics in the X-ray beam were minimized by detuning the Si(111) double-crystal monochromator by 15–20% at the Rh K edge (23,220 eV) or the Ir L_{III} edge (11,215 eV).

In the EXAFS experiments, N_2, H_2, or mixtures of H_2 and/or N_2 and/or propene usually passed through traps containing particles of copper and activated zeolite to remove traces of O_2 and moisture and then passed through the EXAFS cell mounted in the beam line. As the gases flowed, EXAFS data were obtained.

X-ray absorption near-edge spectra were also recorded for rhodium foil at room temperature and for the untreated sample formed from the zeolite and $[Rh(CO)_2(acac)]$.

Propene Hydrogenation Catalyzed in an EXAFS Cell

Measurement of Catalytic Activity

Propene hydrogenation catalyzed by zeolite-supported rhodium or iridium clusters or aggregates was carried out at 25°C in an EXAFS cell in the laboratory (not at the synchrotron). The catalysts were pretreated *in situ* prior to the catalysis experiments. Typically, 100 mg of sample was pressed into a self-supporting wafer and loaded into the cell, as was done at the synchrotron for EXAFS experiments. The precursor in each sample was decarbonylated in

TABLE 1

Crystallographic Data Characterizing the Reference Compounds and Fourier Transform Ranges Used in the EXAFS Data Analysis[a]

		Crystallographic data			Fourier transform		
Ref. compd	Shell	N	R (Å)	Ref	Δk (Å^{-1})	Δr (Å)	n
Rh foil	Rh–Rh	12	2.69	20	2.86–19.60	1.62–3.12	3
Rh foil[b]	Rh–Rh	12	2.69	20	4.1–15.8	1.78–2.77	3
RhNa[c]	Rh–Na	1	1.75	This work	1.0–20.0	0–8.0	0
Rh_2O_3	Rh–O	6	2.050	22	2.67–15.69	0.00–2.10	2
$[Ru_3(CO)_{12}]$	Ru–C	4	1.910	23	3.71–14.80	0.95–1.87	1
	Ru–O*	4	3.050	23	3.75–14.80	1.90–3.11	2
Pt foil	Pt–Pt	12	2.77	20	1.9–19.8	1.9–3.0	3
$Na_2Pt(OH)_6$	Pt–O	6	2.05	24	1.4–17.7	0.5–2.0	3
$[Ir_4(CO)_{12}]$	Ir–C	3	1.87	25	2.8–16.5	1.1–2.0	3
	Ir–O*	3	3.01	25	2.8–16.5	2.0–3.3	3
IrAl alloy	Ir–Al[d]	8	2.58	16	2.7–12.0[e]	0.98–2.98	3

[a] Notation: N, coordination number for absorber-backscatterer pair; R, distance; Δk, limits used for forward Fourier transformation (k is the wave vector); Δr, limits used for shell isolation (r is distance); n, power of k used for Fourier transformation.

[b] Room-temperature data; used to analyze *in situ* data for supported Rh clusters.

[c] Calculated with FEFF 4.05.[21]

[d] After subtraction of Ir–Ir contribution: $N = 6$, $R = 2.98$ Å, $\Delta\sigma^2$ (Debye-Waller factor) $= -0.001$ Å^2, ΔE_0 (inner potential correction) $= -3.3$.[26]

[e] A theoretical Ir–Al EXAFS function was calculated with the FEFF program[21] and adjusted to agree with the limited Ir–Al reference data obtained as described here for use of a larger interval in k space for fitting iridium data.[26]

flowing H_2 at a set temperature. A reaction mixture containing H_2 and propene at atmospheric pressure passed through the EXAFS cell (reactor) at a total flow rate of 100 ml/min (NTP); the cell was heated with cartridge heaters, and temperature was controlled within only approximately $\pm 5^\circ$C. The effluent gas mixture was analyzed with an on-line Hewlett-Packard gas chromatograph (HP-5890, Series II) equipped with a DB-624 capillary column (J&W Scientific) and a flame ionization detector.

The volume of the cell was about 125 ml, and the gas flow rate was about 100 ml/min, giving an average residence time of about 1 min. The dimensions of the catalyst wafer were approximately $1 \times 4 \times 16$ mm. The mixture of propene, H_2, and N_2 flowed largely around the wafer (rather than through it) and through the space between the sample holder and the cell block. The zeolite powder is characterized by an average particle size of about 5 μm.

EXAFS Data Analysis

EXAFS Reference Data

The EXAFS data were analyzed with experimentally determined reference files (16, 17). The parameters used to extract these files are summarized in Table 1. Details of the preparation of the reference files are presented elsewhere (11, 27).

TABLE 2

EXAFS Results Characterizing NaY Zeolite-Supported Rhodium or Iridium Carbonyl Clusters[a]

		Conditions in cell during scan				EXAFS parameters			
Metal carbonyl cluster	Support pretreatment[b, c]	% Propylene	% H_2	Temp (°C)	Backscatterer	N	R (Å)	$\Delta\sigma^2$ (Å^2)	ΔE_0 (eV)
$[Rh_6(CO)_{16}]$	Yes	0	0	−150	Rh	3.3	2.76	0.00050	2.3
$[Rh_6(CO)_{16}]$	No	0	0	−150	Rh	3.8	2.76	−0.00020	4.0
$[Ir_4(CO)_{12}]$	Yes	0	0	−150	Ir	2.6	2.70	0.00105	2.0
$[Ir_6(CO)_{16}]$	Yes	0	0	−150	Ir	3.3	2.68	0.00155	0.44

[a] Samples were scanned under vacuum. Notation: R, absorber backscatterer distance. Other terms defined in Table 1.

[b] If no, the support was evacuated at room temperature for 12 h (following gas treatment for samples treated in O_2).

[c] If yes, the support was calcined by flowing O_2 over the support at 300°C, followed by evacuation at 300°C for 12 h.

TABLE 3

EXAFS Results Characterizing NaY Zeolite-Supported Rhodium and Iridium Clusters or Aggregates[a]

Catalyst pretreatment conditions			Conditions during scan[d]				EXAFS parameters				Cluster or aggregate
Treatment gas/ Precursor	Temp (°C)	Support pretreatment[b,c]	% Propene	% H_2	Temp (°C)	Backscatterer[e,f]	N	R (Å)	$\Delta\sigma^2$ (Å^2)	ΔE_0 (eV)	
H_2/[$Rh_6(CO)_{16}$]	200	Yes	0	0	25	Rh	3.2	2.69	0.00366	3.7	Cluster
						O	2.0	2.19	0.01500	−6.6	
						C	4.0	1.99	0.01500	−14.2	
H_2/[$Rh_6(CO)_{16}$]	250	No	0	0	25	Rh	5.9	2.67	0.00264	6.1	Aggregate
						O	0.8	2.12	0.00367	−1.2	
						C	1.0	1.87	0.00707	19.5	
H_2/[$Ir_4(CO)_{12}$]	300	Yes	0	0	25	Ir	3.2	2.69	0.00404	−0.4	Cluster
						O	1.3	2.26	0.00357	−14.0	
						C	2.7	1.97	0.01500	−14.5	
H_2/[$Ir_6(CO)_{16}$]	300	Yes	0	0	25	Ir	4.6	2.68	0.00493	−0.3	Aggregate
						O	2.2	2.21	0.00031	−3.8	
						C	2.0	1.96	0.01500	−6.1	

[a] Notation as in Table 2.
[b] If no, the support was evacuated at room temperature for 12 h (following gas treatment for samples treated in O_2).
[c] If yes, the support was calcined by flowing O_2 over the support at 300°C, followed by evacuation at 300°C for 12 h.
[d] The samples were scanned under vacuum.
[e] For rhodium samples, an additional long Rh–O contribution was fitted (typical values: $N = 1.7$, $R = 3.0$ Å, $\Delta\sigma^2 = -0.004$ Å^2, $\Delta E_0 = -10$ eV).
[f] Additionally, a long Ir–O contribution (typical values: $N = 0.5$, $R = 2.8$ Å, $\Delta\sigma^2 = -0.003$ Å^2, $\Delta E_0 = -20$ eV) and an Ir–Al contribution (typical values: $N = 0.1$, $R = 1.5$ Å, $\Delta\sigma^2 = -0.002$ Å^2, $\Delta E_0 = 20$ eV) were fitted.

TABLE 4

EXAFS Results Characterizing NaY Zeolite-Supported Rhodium and Iridium Clusters or Aggregates in the Presence of H_2[a]

Catalyst pretreatment conditions			Conditions during scan[d]				EXAFS parameters				Cluster or aggregate
Treatment gas/ Precursor	Temp (°C)	Support pretreatment[b,c]	% Propene	% H_2	Temp (°C)	Backscatterer[e,f]	N	R (Å)	$\Delta\sigma^2$ (Å^2)	ΔE_0 (eV)	
H_2/[$Rh_6(CO)_{16}$]	200	Yes	0	6	25	Rh	2.9	2.71	0.00316	−3.4	Cluster
						O	0.6	2.28	−0.00340	−20.0	
						C	3.4	2.01	0.01500	−14.4	
H_2/[$Rh_6(CO)_{16}$]	250	No	0	6	25	Rh	5.3	2.68	0.00295	5.6	Aggregate
						O	1.6	2.12	0.00561	−4.5	
						C	0.7	1.95	0.00036	−11.5	
H_2/[$Ir_4(CO)_{12}$]	300	Yes	0	6	25	Ir	3.3	2.70	0.00420	1.6	Cluster
						O	1.5	2.26	0.00498	−14.2	
						C	2.9	1.98	0.01500	−16.7	
H_2/[$Ir_6(CO)_{16}$]	300	Yes	0	6	25	Ir	4.6	2.69	0.00509	0.44	Aggregate
						O	0.9	2.23	0.00049	−3.4	
						C	3.0	1.97	0.01500	−6.9	

[a] Notation as in Table 2.
[b] If no, the support was evacuated at room temperature for 12 h (following gas treatment for samples treated in O_2).
[c] If yes, the support was calcined by flowing O_2 over the support at 300°C, followed by evacuation at 300°C for 12 h.
[d] The samples under vacuum were scanned.
[e] For rhodium samples, an additional long Rh–O contribution was fitted (typical values: $N = 1.7$, $R = 3.0$ Å, $\Delta\sigma^2 = -0.004$ Å^2, $\Delta E_0 = -10$ eV).
[f] Additionally, a long Ir–O contribution (typical values: $N = 0.5$, $R = 2.8$ Å, $\Delta\sigma^2 = -0.003$ Å^2, $\Delta E_0 = -20$ eV) and an Ir–Al contribution (typical values: $N = 0.1$, $R = 1.5$ Å, $\Delta\sigma^2 = -0.002$ Å^2, $\Delta E_0 = 20$ eV) were fitted.

TABLE 5

EXAFS Results Characterizing NaY Zeolite-Supported Rhodium and Iridium Clusters or Aggregates in the Presence of Propene[a]

Catalyst pretreatment conditions			Conditions during scan[d]				EXAFS parameters				Cluster or Aggregate
Treatment gas/ Precursor	Temp (°C)	Support pretreatment[b,c]	% Propene	% H_2	Temp (°C)	Backscatterer[e,f]	N	R (Å)	$\Delta\sigma^2$ (Å^2)	ΔE_0 (eV)	
H_2/[$Rh_6(CO)_{16}$]	200	Yes	6	0	25	Rh	3.2	2.67	0.00361	6.2	Cluster
						O	1.0	2.26	0.00241	−16.7	
						C	3.6	2.02	0.01500	−15.6	
H_2/[$Rh_6(CO)_{16}$]	250	No	6	0	25	Rh	5.4	2.65	0.00343	8.3	Aggregate
						O	1.3	2.11	0.00307	−5.3	
						C	0.7	1.95	−0.00173	−9.8	
H_2/[$Ir_4(CO)_{12}$]	300	Yes	3	0	25	Ir	3.8	2.67	0.00499	3.2	Cluster
						O	1.2	2.21	0.00244	−3.4	
						C	3.3	1.97	0.01447	−10.8	
H_2/[$Ir_6(CO)_{16}$]	300	Yes	6	0	25	Ir	4.7	2.66	0.00530	2.0	Aggregate
						O	1.2	2.22	0.00241	−1.4	
						C	2.7	1.99	0.01042	−7.5	

[a] Notation as in Table 2.
[b] If no, the support was evacuated at room temperature for 12 h (following gas treatment for samples treated in O_2).
[c] If yes, the support was calcined by flowing O_2 over the support at 300°C, followed by evacuation at 300°C for 12 h.
[d] When the sample was not under vacuum, the balance of the gas phase was N_2.
[e] For rhodium samples, an additional long Rh–O contribution was fitted (typical values: $N = 1.7$, $R = 3.0$ Å, $\Delta\sigma^2 = -0.004$ Å^2, $\Delta E_0 = -10$ eV).
[f] Additionally, a long Ir–O contribution (typical values: $N = 0.5$, $R = 2.8$ Å, $\Delta\sigma^2 = -0.003$ Å^2, $\Delta E_0 = -20$ eV) and an Ir–Al contribution (typical values: $N = 0.1$, $R = 1.5$ Å, $\Delta\sigma^2 = -0.002$ Å^2, $\Delta E_0 = 20$ eV) were fitted.

Data Characterizing Zeolite-Supported Rhodium Carbonyls and Iridium Carbonyls

Details of the analyses of the EXAFS data characterizing the supported iridium carbonyl clusters and rhodium carbonyl clusters are presented elsewhere (16, 17). The uncertainties in the EXAFS parameters are estimated to be approximately the following (where M is Rh or Ir): M–M first-shell coordination numbers, ±20%; M–M near-neighbor distances, ±1%; M–low-Z scatterer coordination numbers, ±50%; M–low-Z scatterer distances, ±10%. Because of the relatively large uncertainties in the M–low-Z parameters, the low-Z scatterers cannot all be identified with confidence.

Data Characterizing Decarbonylated Samples Formed from Rhodium Carbonyls

EXAFS data from two to six scans were averaged for each sample. The normalized EXAFS functions were obtained from the averaged X-ray absorption spectra by a cubic spline background subtraction and normalized by division by the edge height (e.g., Fig. 1A). In the intermediate and higher ranges of the wave vector k ($8 < k < 12$ Å^{-1}), there are strong oscillations characteristic of metal–metal interactions in each sample, consistent with the presence of metal clusters or particles.

No attempt was made to smooth the EXAFS data; a difference file technique (28, 29) was used to extract the EXAFS parameters. EXAFS data characterizing clusters formed by decarbonylation in the presence of H_2 were fitted with Rh–Rh, Rh–$O_{support}$, Rh–C, and Rh–O* contributions (where O* refers to carbonyl oxygen). Furthermore, when the sample contained aggregated rhodium, second and third Rh–Rh shells were fitted, at distances of about 3.8 and 4.65 Å, respectively. The number of parameters used to fit the data in these main-shell analyses was 16 or 24. The statistically justified number n was estimated to be approximately 33 for each sample; the estimate is based on the Nyquist theorem (30), $n = (2\Delta k \Delta r/\pi) + 1$, where r is the metal-scatterer distance, and Δk and Δr, respectively, are the k and r ranges used in the forward and inverse Fourier transformations (Δk and Δr are about 10 Å^{-1} and 5 Å, respectively). Details of the method are presented elsewhere (17).

Data Characterizing Decarbonylated Samples Formed from Iridium Carbonyls

EXAFS data from two to six scans were averaged for each sample. The normalized EXAFS functions were obtained as stated above (e.g., Fig. 2A). In the intermediate and higher k ranges ($8 < k < 16$ Å^{-1}), oscillations characteristic of metal–metal interactions were found for each sample.

Using methods described elsewhere (14, 16), the EXAFS data characterizing clusters formed by decarbonylation in H_2 were fitted with Ir–Ir, Ir–C, Ir–Al, and two Ir–O contributions. The number of fitting parameters in these main-shell analyses was 20; the statistically justified number is approximately 36 for each sample.

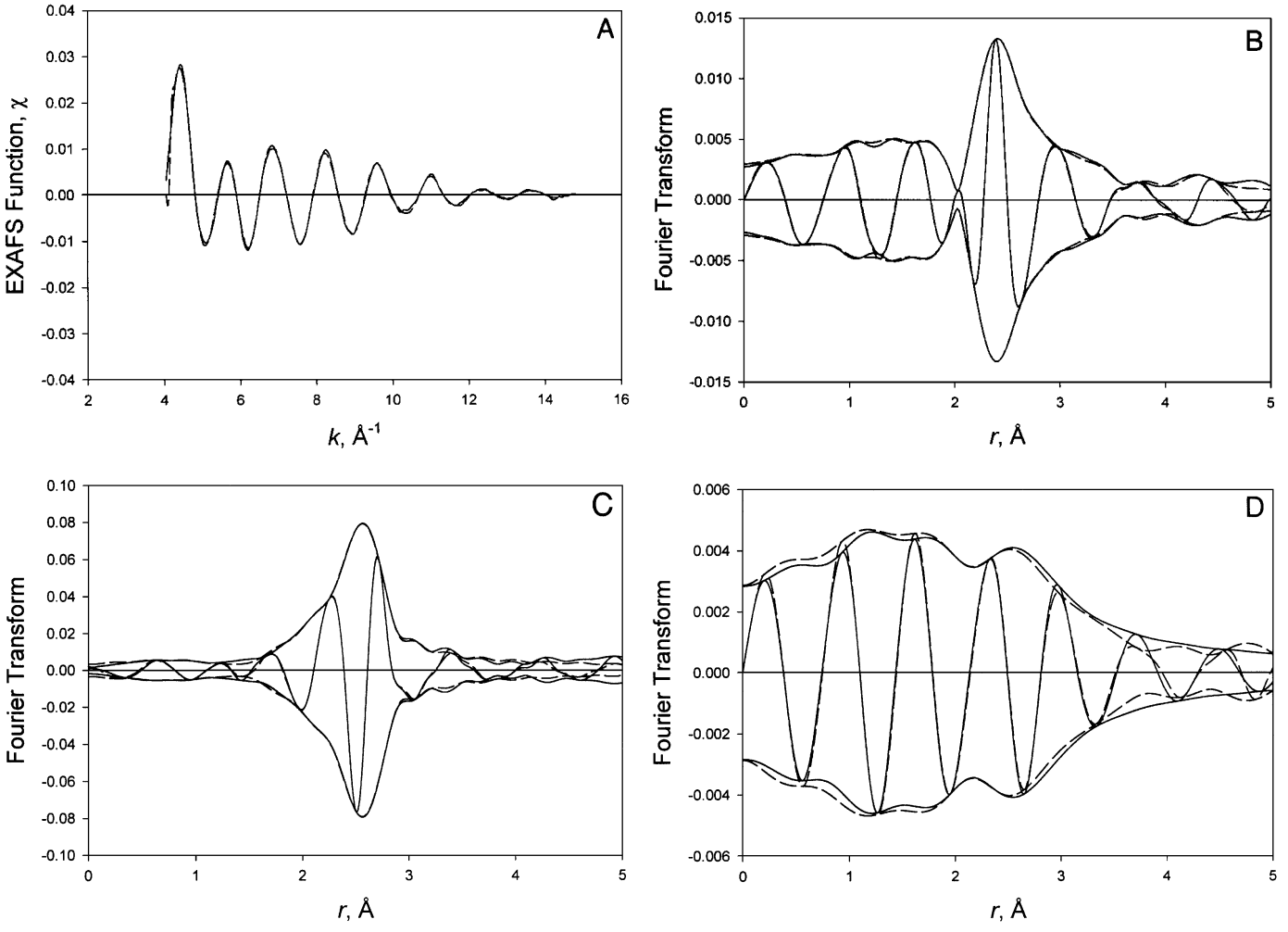

FIG. 1. Results of EXAFS analysis characterizing the sample formed by treatment of $[Rh_6(CO)_{16}]$ supported in zeolite Y in H_2 at 250°C: (A) Raw EXAFS function (solid line) and sum of the calculated Rh–Rh + Rh–O_s + Rh–C + Rh–O* contributions (dashed line). (B) Imaginary part and magnitude of Fourier transform (unweighted, $\Delta k = 4.1$–14.6 Å^{-1}) of raw EXAFS function (solid line) and sum of the calculated Rh–Rh + Rh–O_s + Rh–C + Rh–O_l contributions (dashed line). (C) Residual spectrum illustrating the Rh–Rh contribution; imaginary part and magnitude of Fourier transform (unweighted, Rh–Rh phase and amplitude corrected, $\Delta k = 4.1$–14.6 Å^{-1}) of raw EXAFS data minus calculated Rh–O_s + Rh–C + Rh–O_l contributions (solid line) and calculated Rh–Rh contribution (dashed line). (D) Residual spectrum illustrating the Rh–low-Z backscatterer interactions; imaginary part and magnitude of Fourier transform (unweighted, $\Delta k = 4.1$–10 Å^{-1}) of raw EXAFS data minus calculated Rh–Rh contribution (solid line) and calculated Rh–O_s + Rh–C + Rh–O_l contributions (dashed line).1

RESULTS

Infrared Evidence of Formation of Zeolite-Supported Rhodium Carbonyl Clusters and Iridium Carbonyl Clusters

When $[Rh(CO)_2(acac)]$ in *n*-pentane solution was brought in contact with the uncalcined or calcined zeolite, the infrared spectra of the solid matched those (17) indicating rhodium dicarbonyls (31–34). Treatment of the sample formed from $[Rh(CO)_2(acac)]$ in uncalcined or in calcined zeolite in flowing CO at 125°C for 12 h gave a spectrum consistent with $[Rh_6(CO)_{16}]$ (35–37); details are given elsewhere (17).

Similarly, the precursor $[Ir(CO)_2(acac)]$ in *n*-pentane solution in contact with calcined zeolite gave samples with spectra indicative of iridium dicarbonyls (38, 39). Treatment of the sample in CO at 40 or 175°C for 12 h gave samples with infrared spectra consistent with $[Ir_4(CO)_{12}]$ or $[Ir_6(CO)_{16}]$ (both isomers (40)), respectively.

EXAFS Evidence of Zeolite-Supported Rhodium Carbonyls and Iridium Carbonyls

The EXAFS data (not shown) characterizing the samples formed from the uncalcined and from the calcined zeolite containing $[Rh(CO)_2(acac)]$ under vacuum at about −150°C, following treatment in CO, show oscillations up to *k* values of about 16 Å^{-1}, consistent with Rh–Rh contributions (Table 2).

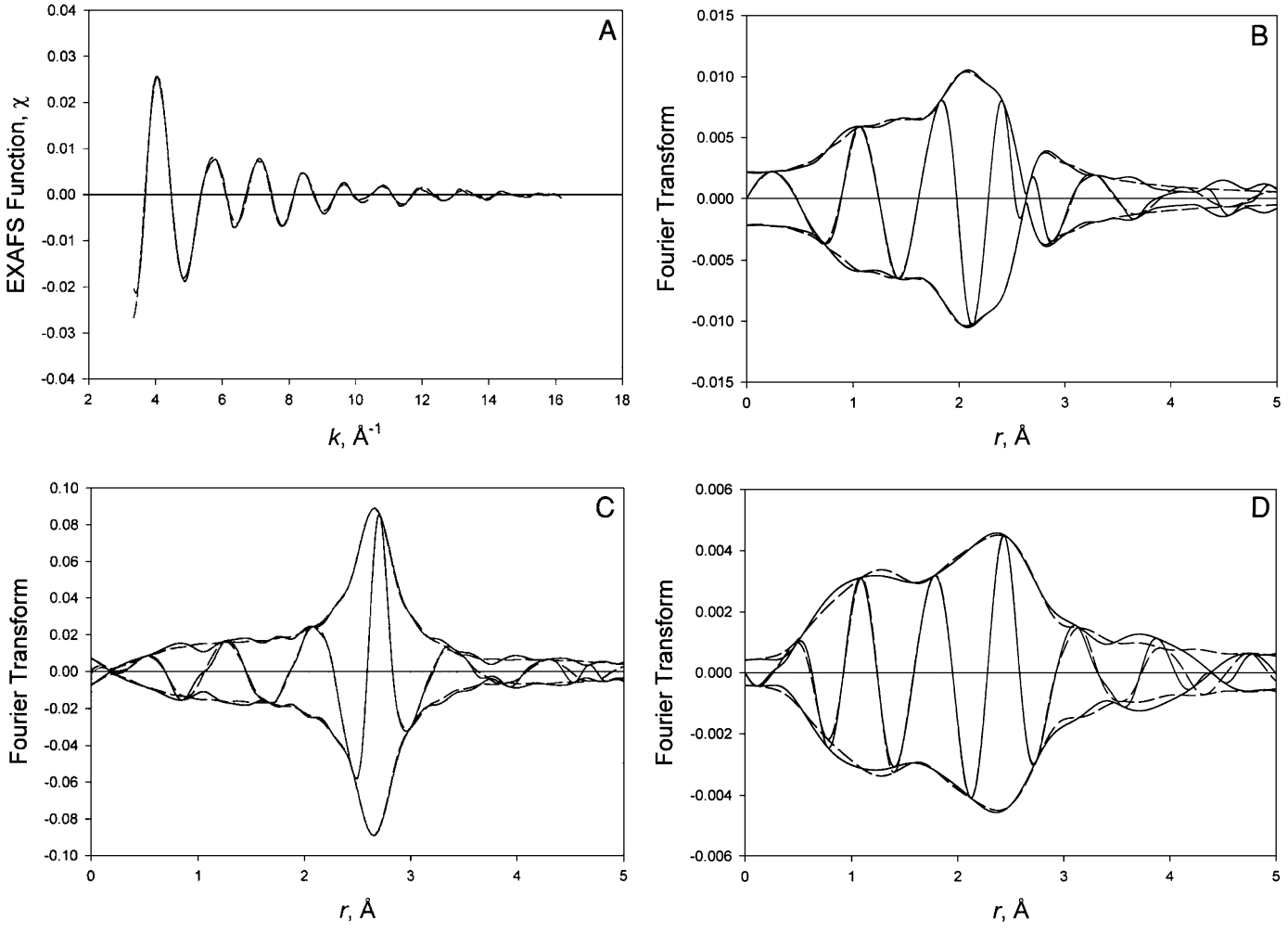

FIG. 2. Results of EXAFS analysis characterizing the sample formed by treatment of $[Ir_4(CO)_{12}]$ supported in the calcined zeolite in H_2 at 300°C: (A) Raw EXAFS function (solid line) and sum of the calculated Ir–Ir + Ir–O_s + Ir–C + Ir–O_l + Ir–Al contributions (dashed line). (B) Imaginary part and magnitude of Fourier transform (unweighted, $\Delta k = 4.1$–14.6 Å^{-1}) of raw EXAFS function (solid line) and sum of the calculated Ir–Ir + Ir–O_s + Ir–C + Ir–O_l + Ir–Al contributions (dashed line). (C) Residual spectrum illustrating the Ir–Ir contribution; imaginary part and magnitude of Fourier transform (unweighted, Ir–Ir phase- and amplitude-corrected, $\Delta k = 4.1$–14.6 Å^{-1}) of raw EXAFS data minus calculated Ir–O_s + Ir–C + Ir–O_l + Ir–Al contributions (solid line) and calculated Rh–Rh contribution (dashed line). (D) Residual spectrum illustrating the Ir–low–Z backscatterer interactions; imaginary part and magnitude of Fourier transform (unweighted, $\Delta k = 4.1$–10 Å^{-1}) of raw EXAFS data minus calculated Ir–Ir contribution (solid line) and calculated Ir–O_s + Ir–C + Ir–O_l + Ir–Al contributions (dashed line).

The EXAFS data (not shown) characterizing the samples formed from the calcined zeolite containing $[Ir(CO)_2(acac)]$, following treatment in CO at 40 or 175°C, show oscillations up to k values of about 16 Å^{-1}, consistent with Ir–Ir contributions. The fits of the Ir–Ir first-shell contributions are presented in Table 2; additional fitting parameters are not presented; such results are available for similar samples (16).

EXAFS Evidence of Partially Decarbonylated Rhodium Clusters and Aggregates

The EXAFS data characterizing the decarbonylated rhodium clusters scanned under vacuum and formed by treatment of the calcined zeolite-supported $[Rh_6(CO)_{16}]$ in H_2 at 200°C for 2 h or by treatment of the uncalcined zeolite-supported $[Rh_6(CO)_{16}]$ in H_2 at 250°C for 2 h show oscillations up to k values equal to about 16 Å^{-1}, consistent with Rh–Rh contributions and rhodium clusters or aggregates, respectively, in the zeolite (Fig. 1).

The EXAFS data characterizing the sample formed by treatment of the calcined zeolite-supported $[Rh_6(CO)_{16}]$ in H_2 at 200°C for 2 h were fitted satisfactorily by a Rh–Rh contribution, at 2.67 Å, and Rh–low-Z contributions, approximated as a short Rh–O (2.1 Å), Rh–O* (3.0 Å), and Rh–C (1.97 Å). The Rh–Rh first-shell coordination number, 3.3, is nearly equal to that of the rhodium carbonyl precursor. These results suggest that partially decarbonylated

clusters formed with almost no change in the metal framework nuclearity. Therefore, we infer that the clusters were approximately hexarhodium, on average. The partially decarbonylated clusters had significantly fewer CO ligands than the metal carbonyl precursor, as shown by infrared spectroscopy (17).

To illustrate the goodness of the fits, comparisons of the raw data and the fits in *k* space and in *r* space are shown in Figs. 1A and 1B, respectively, for the clusters formed by the treatment of zeolite-supported $[Rh_6(CO)_{16}]$ in H_2 at 200°C. A comparison of the residual spectrum formed by subtraction of Rh–low-Z contributions from the raw EXAFS functions with that of the fitted Rh–Rh contribution is shown in Fig. 1C. Subtraction of the Rh–Rh contribution from the EXAFS function gives a residual spectrum that includes any metal-support interactions as well as higher-shell Rh–Rh contributions. Because the infrared data show that the clusters were not fully decarbonylated, the residual spectrum was fitted for $Rh–O_{support}$, Rh–C, and one Rh–O* contributions. The sum of the contributions is compared with the appropriate residual spectrum in Fig. 1D. These comparisons show that both the Rh–Rh and Rh–low-Z contributions were fitted satisfactorily; however, the data are not sufficient to identify the low-Z scatterers with confidence (17).

The EXAFS data representing partially decarbonylated rhodium aggregates (characterized by infrared spectroscopy (17)) supported on uncalcined NaY zeolite and formed by treatment of $[Rh_6(CO)_{16}]$ in H_2 at 250°C for 2 h were fitted satisfactorily by a Rh–Rh contribution, at 2.67 Å, and Rh–low-Z contributions, approximated as a short Rh–O (2.1 Å), Rh–O* (3.0 Å), and Rh–C (1.97 Å). The Rh–Rh first-shell coordination number, 5.9, is considerably larger than the value characterizing the rhodium carbonyl precursor (3.8); the EXAFS data also indicate second- and third-shell Rh–Rh contributions (at distances of 3.8 and 4.68 Å, respectively). Thus, these results indicate that rhodium aggregates formed in the uncalcined zeolite, having approximate nuclearities of 15–20 atoms, on average (41). Infrared spectra (17) show that these aggregates have significantly fewer CO ligands than the clusters described in the preceding paragraph. The *k*-range used in the fitting and the standard deviations in the EXAFS function characterizing each decarbonylated sample were typically 4.2–14.7 $Å^{-1}$ and 0.002, respectively. The EXAFS parameters estimated in the data fitting are given in Table 3.

To summarize, the data show that treatment of calcined zeolite-supported $[Rh_6(CO)_{16}]$ in H_2 at 200°C led to the formation of clusters consisting of approximately 6 atoms each, on average. The clusters had significantly fewer CO ligands than the precursor rhodium carbonyl. Henceforth, we refer to the sample containing supported rhodium clusters to contrast it to the sample formed by treatment of uncalcined zeolite-supported $[Rh_6(CO)_{16}]$ in H_2 at 250°C, which incorporated rhodium entities having 15–20 atoms each, on average, with few CO ligands, which we refer to as aggregates.

EXAFS Evidence of Iridium Clusters

The EXAFS data representing the samples scanned under vacuum at −150°C and formed by treatment of the calcined zeolite-supported $[Ir_4(CO)_{12}]$ in H_2 at 300°C for 2 h or by treatment of the calcined zeolite-supported $[Ir_6(CO)_{16}]$ in H_2 at 300°C for 2 h show oscillations up to values of *k* equal to about 16 $Å^{-1}$, consistent with iridium clusters or aggregates (Fig. 2).

Because infrared spectra indicate that the iridium clusters (or aggregates) had been fully decarbonylated (15, 16), we represent the EXAFS data with Ir–Ir first-shell and Ir–low-Z contributions not including Ir–O*. The Ir scatterers are identified with confidence, but the low-Z scatterers are not; candidates include O, Al, Si, Na, and C (the O and C from possibly unconverted acac ligands, products of decarbonylation, and/or traces of residual solvent).

The averaged data representing the sample formed by treatment of the calcined zeolite-supported $[Ir_4(CO)_{12}]$ in H_2 at 300°C for 2 h were fitted satisfactorily by the Ir–Ir contribution and others approximated as a short Ir–O (2.1 Å), long Ir–O (2.8 Å), Ir–C (1.97 Å), and (a tentatively identified) Ir–Al (1.5 Å). The *k*-range used in the fitting and the standard deviations in the EXAFS function for each decarbonylated sample were typically 4.2–14.6 $Å^{-1}$ and 0.002, respectively. The EXAFS parameters determined in the fitting are summarized in Table 3. The Ir–Ir first-shell coordination number, 3.2, is slightly larger than that of the precursor iridium carbonyl (2.6). This result suggests that some of the iridium may have aggregated to form clusters having nuclearities greater than four atoms, with most still being Ir_4. This sample is referred to as containing supported iridium clusters.

Comparisons of the data and the fits in *k* space and in *r* space are shown in Figs. 2A and 2B, respectively, for the clusters formed by treatment of zeolite-supported $[Ir_4(CO)_{12}]$ in H_2 at 300°C. Comparison of the residual spectrum formed by subtraction of Ir–low-Z contributions from the EXAFS function with that of the fitted Ir–Ir contribution is shown in Fig. 2C. The residual spectrum was fitted with an $Ir–O_{support}$, a long Ir–O, and an Ir–C contribution. The sum of the contributions is compared with the appropriate residual spectrum in Fig. 2D; the comparison shows that the Ir–Ir and Ir–low-Z contributions were fitted satisfactorily.

The data representing the sample formed by the treatment of the calcined zeolite-supported $[Ir_6(CO)_{16}]$ in H_2 at 300°C for 2 h were fitted satisfactorily by an Ir–Ir contribution and others approximated as a short Ir–O (2.1 Å), long Ir–O (2.8 Å), Ir–C (1.97 Å), and (a tentatively identified)

Ir–Al (1.5 Å). The EXAFS parameters are summarized in Table 3. The Ir–Ir first-shell coordination number (4.6) is significantly larger than that of the precursor iridium carbonyl (3.3), indicating some aggregation of the iridium, with the resulting aggregates having about 10 atoms each, on average (41).

To summarize, when calcined zeolite-supported $[Ir_4(CO)_{12}]$ was decarbonylated in H_2 at 300°C, the Ir–Ir first-shell coordination number increased from 2.6 to 3.2, indicating that the metal may have aggregated slightly to form clusters having about four atoms each, on average. When $[Ir_6(CO)_{16}]$ was decarbonylated under the same conditions, aggregates of about 10 atoms each, on average, formed, as shown by an increase of the Ir–Ir first-shell coordination number from 3.3 to 4.6.

EXAFS Characterization of Supported Metal Clusters and Aggregates in Various Atmospheres

The following section includes EXAFS results representing the several samples in various atmospheres. For brevity, only a few results are stated in addition to the parameter values given in tables.

Partially decarbonylated rhodium clusters or aggregates were scanned at room temperature in the presence of 6% H_2 in N_2. The data representing the rhodium clusters, now expected to include adsorbed hydrogen, were fitted satisfactorily by a Rh–Rh contribution, at about 2.71 Å, and Rh–low-Z contributions (Table 4; Figs. 3A and 3B). The data characterizing rhodium aggregates indicate first-, second-, and third-shell Rh–Rh contributions (Table 4; Figs. 4A and

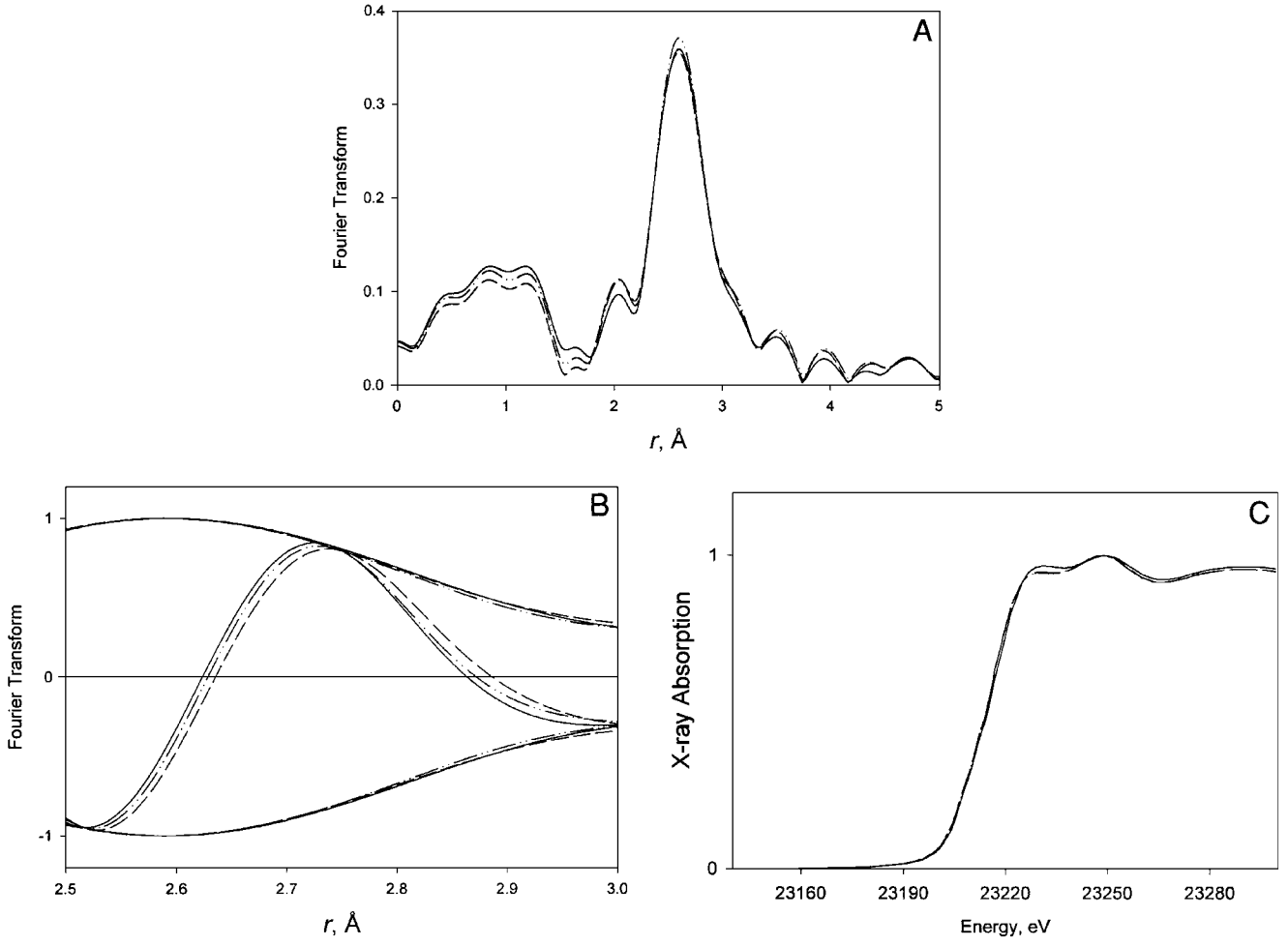

FIG. 3. Comparison of the X-ray absorption data characterizing supported rhodium clusters formed by treatment of $[Rh_6(CO)_{16}]$ supported in the calcined zeolite in H_2 at 200°C: (A) Magnitude of Fourier transform (k^0-weighted, Rh–Rh phase- and amplitude-corrected) of EXAFS data characterizing sample with gas flowing through the cell containing H_2 and propene in N_2 carrier gas with compositions of (0% H_2, 6% propene) (solid line), (2% H_2, 2% propene) (dotted-dashed line), and (6% H_2, 0% propene) (dashed line). (B) Scaled imaginary part and magnitude of Fourier transform (k^0-weighted, Rh–Rh phase- and amplitude-corrected) of EXAFS data characterizing sample with gas flowing through the cell containing H_2 and propene in N_2 carrier gas with compositions of (0% H_2, 6% propene) (solid line), (2% H_2, 2% propene) (dotted-dashed line), and (6% H_2, 0% propene) (dashed line). (C) XANES characterizing sample with gas flowing through the cell containing H_2 and propene in N_2 carrier gas with compositions of (0% H_2, 6% propene) (solid line), (2% H_2, 2% propene) (dotted-dashed line), and (6% H_2, 0% propene) (dashed line).

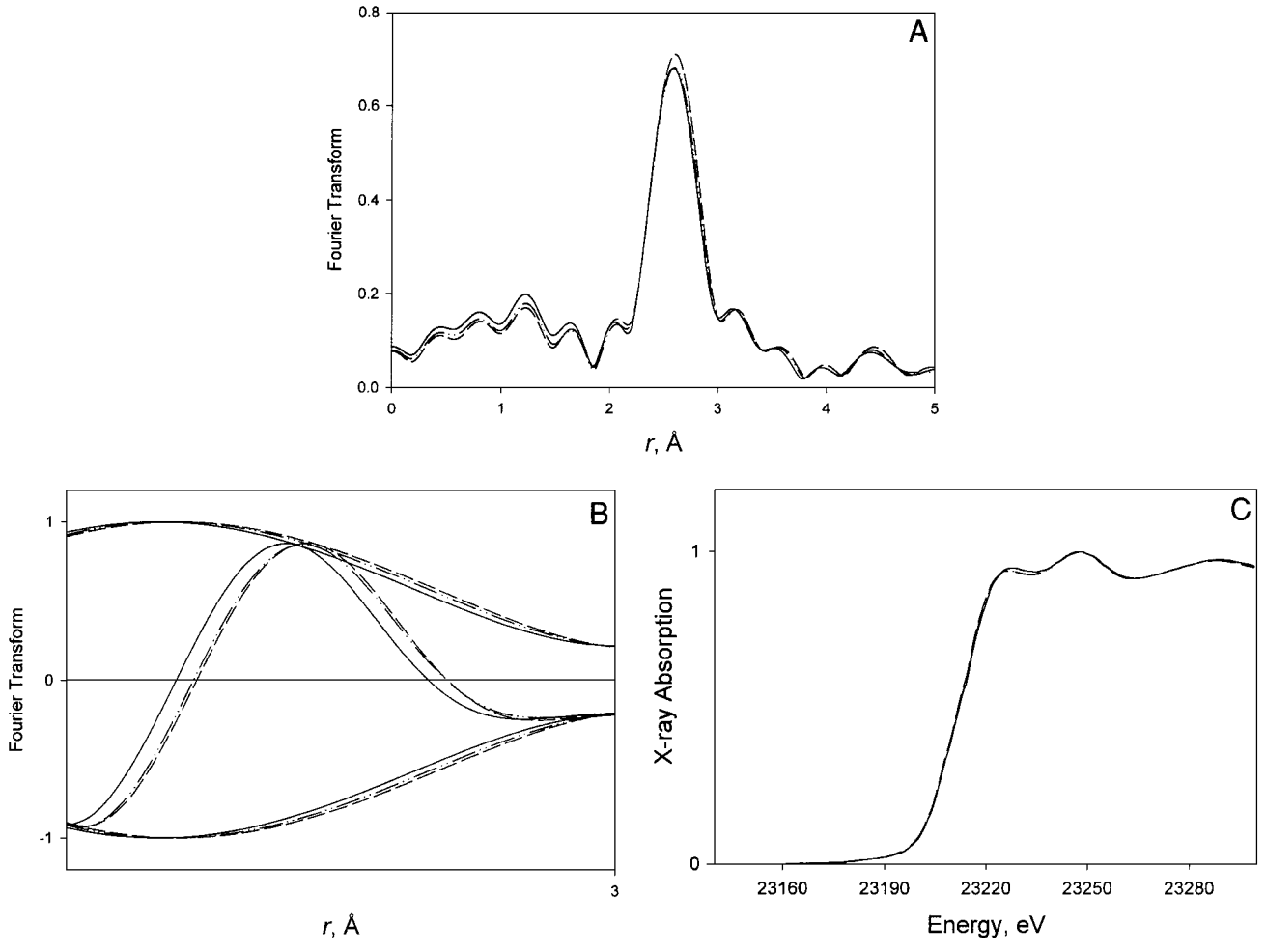

FIG. 4. Comparison of the X-ray absorption data characterizing supported rhodium aggregates formed by treatment of $[Rh_6(CO)_{16}]$ supported in the uncalcined zeolite in H_2 at 250°C: (A) Magnitude of Fourier transform (k^0-weighted, Rh–Rh phase- and amplitude-corrected) of EXAFS data characterizing sample with gas flowing through the cell containing H_2 and propene in N_2 carrier gas with compositions of (0% H_2, 6% propene) (solid line), (2% H_2, 2% propene) (dotted-dashed line), and (6% H_2, 0% propene) (dashed line). (B) Scaled imaginary part and magnitude of Fourier transform (k^0-weighted, Rh–Rh phase- and amplitude-corrected) of EXAFS data characterizing sample with gas flowing through the cell containing H_2 and propene in N_2 carrier gas with compositions of (0% H_2, 6% propene) (solid line), (2% H_2, 2% propene) (dotted-dashed line), and (6% H_2, 0% propene) (dashed line). (C) XANES data characterizing sample with gas flowing through the cell containing H_2 and propene in N_2 carrier gas with compositions of (0% H_2, 6% propene) (solid line), (2% H_2, 2% propene) (dotted-dashed line), and (6% H_2, 0% propene) (dashed line).

4B). Results for the samples consisting of decarbonylated iridium clusters or aggregates, scanned at room temperature in 6% H_2 in N_2, are summarized in Table 4, Figs. 5A and 5B, and Figs. 6A and 6B.

These results show that the presence of H_2 in the gas phase (and presumably atomic hydrogen adsorbed on the metal) did not substantially affect the framework structures of the supported clusters or aggregates of either iridium or rhodium, as shown by the lack of significant changes in the metal–metal first-shell coordination number resulting from the introduction of H_2.

Similar conclusions follow from the results characterizing the samples scanned at room temperature in the presence of 6% propene in N_2 (Table 5). Comparison of the parameters fitting the Rh–Rh contributions of clusters (or aggregates) in propene (Table 5) and those of the same clusters (or aggregates) in H_2 (Table 4) shows a slightly shorter Rh–Rh bonding distance (by about 0.04 Å) in the presence of propene. The shorter Rh–Rh distance is also evident from a comparison of the imaginary parts of the Fourier transforms of the raw EXAFS data (Figs. 3B and 4B). The imaginary part of the Fourier transform representing clusters or aggregates in propene is generally shifted slightly to shorter distances relative to that characterizing the clusters or aggregates in H_2.

The data representing the decarbonylated iridium clusters or aggregates scanned at room temperature in propene (Figs. 5A and 5B and Figs. 6A and 6B, respectively) were fitted satisfactorily with an Ir–Ir contribution and Ir–low-Z contributions (Table 5). Comparison of the parameters

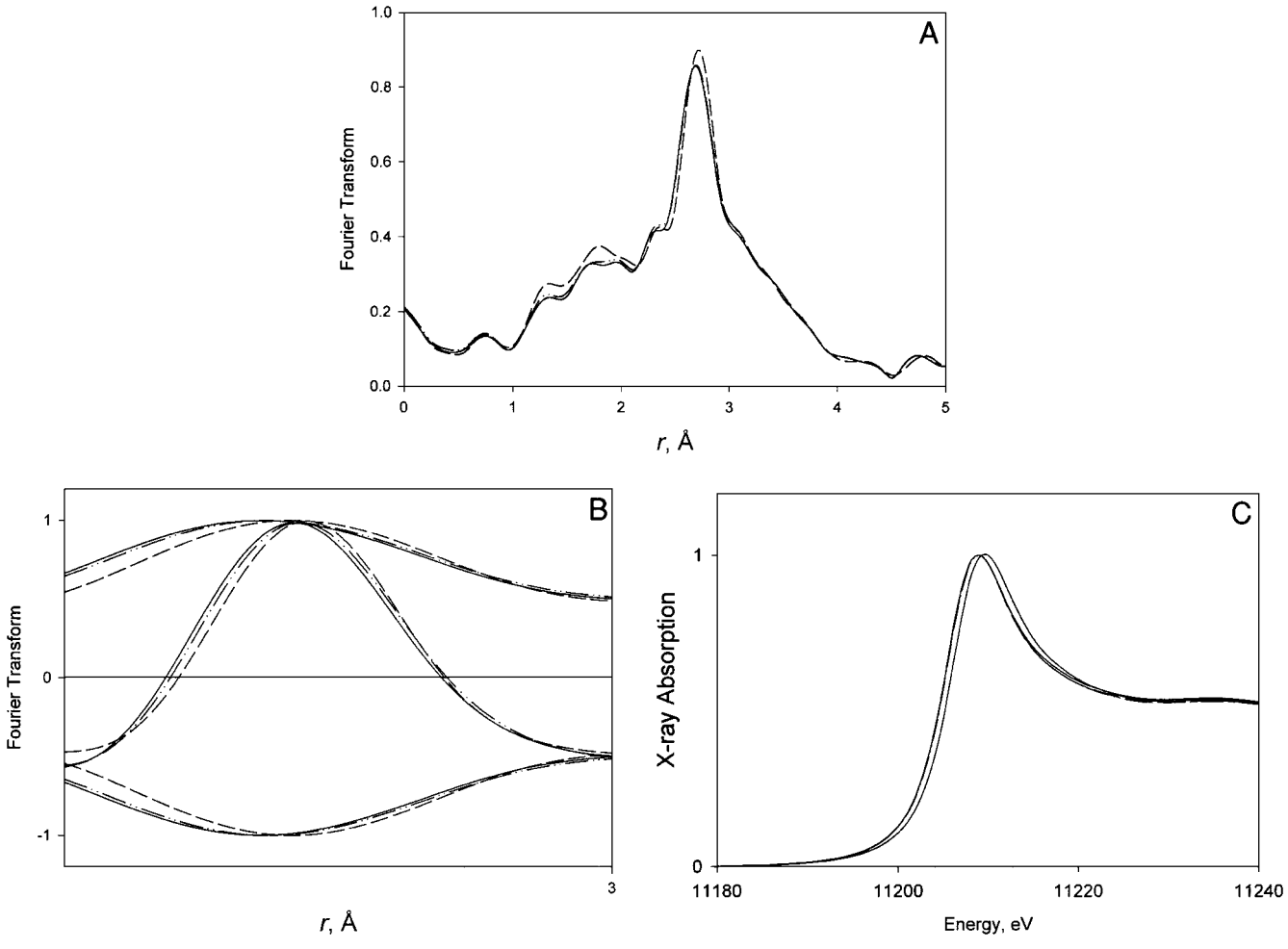

FIG. 5. Comparison of the X-ray absorption data characterizing supported iridium clusters formed by treatment of $[Ir_4(CO)_{12}]$ supported in the uncalcined zeolite in H_2 at 300°C: (A) Magnitude of Fourier transform (k^0-weighted, Ir–Ir phase- and amplitude-corrected) of EXAFS data characterizing sample with gas flowing through the cell containing H_2 and propene in N_2 carrier gas with compositions of (0% H_2, 6% propene) (solid line), (2% H_2, 2% propene) (dotted-dashed line), and (6% H_2, 0% propene) (dashed line). (B) Scaled imaginary part and magnitude of Fourier transform (k^0-weighted, Ir–Ir phase- and amplitude-corrected) of EXAFS data characterizing sample with gas flowing through the cell containing H_2 and propene in N_2 carrier gas with compositions of (0% H_2, 6% propene) (solid line), (2% H_2, 2% propene) (dotted-dashed line), and (6% H_2, 0% propene) (dashed line). (C) XANES data characterizing sample with gas flowing through the cell containing H_2 and propene in N_2 carrier gas with compositions of (0% H_2, 6% propene) (solid line), (2% H_2, 2% propene) (dotted-dashed line), and (6% H_2, 0% propene) (dashed line).

fitting the Ir–Ir contribution characterizing the clusters (or aggregates) in propene and those characterizing the same clusters (or aggregates) in H_2 shows a slightly shorter Ir–Ir distance (by about 0.03 Å) in the former. This result is supported by the imaginary parts of the Fourier transforms of the raw EXAFS data (Figs. 5B and 6B). These results are qualitatively in agreement with the results stated above for rhodium.

Supported Metal Clusters and Aggregates in the Presence of Reacting H_2 and Propene

With propene and H_2 flowing through the EXAFS cell in a 1 : 1 molar ratio at 25°C and catalytic hydrogenation of propene occurring, the partially decarbonylated clusters and aggregates of rhodium were characterized by EXAFS spectra fitted by a Rh–Rh contribution and Rh–low-Z contributions (Table 6). The data representing the rhodium aggregates indicate both second- and third-shell Rh–Rh contributions (at distances of about 3.8 and 4.68 Å, respectively). The *k*-range used in the fitting and the standard deviations in the EXAFS function were typically 4.2–14.7 $Å^{-1}$ and 0.002, respectively. The data indicate no significant differences between the Rh–Rh first-shell coordination number and bonding distance characterizing the rhodium clusters (or aggregates) in the presence of H_2/propene (Table 6; Figs. 3A and 4A) relative to those of the same clusters (or aggregates) in H_2 only (Table 4; Figs. 3A and 4A).

Similarly, with propene and H_2 flowing through the EXAFS cell in a 4 : 1, a 1 : 1, or a 1 : 4 molar ratio at 25°C

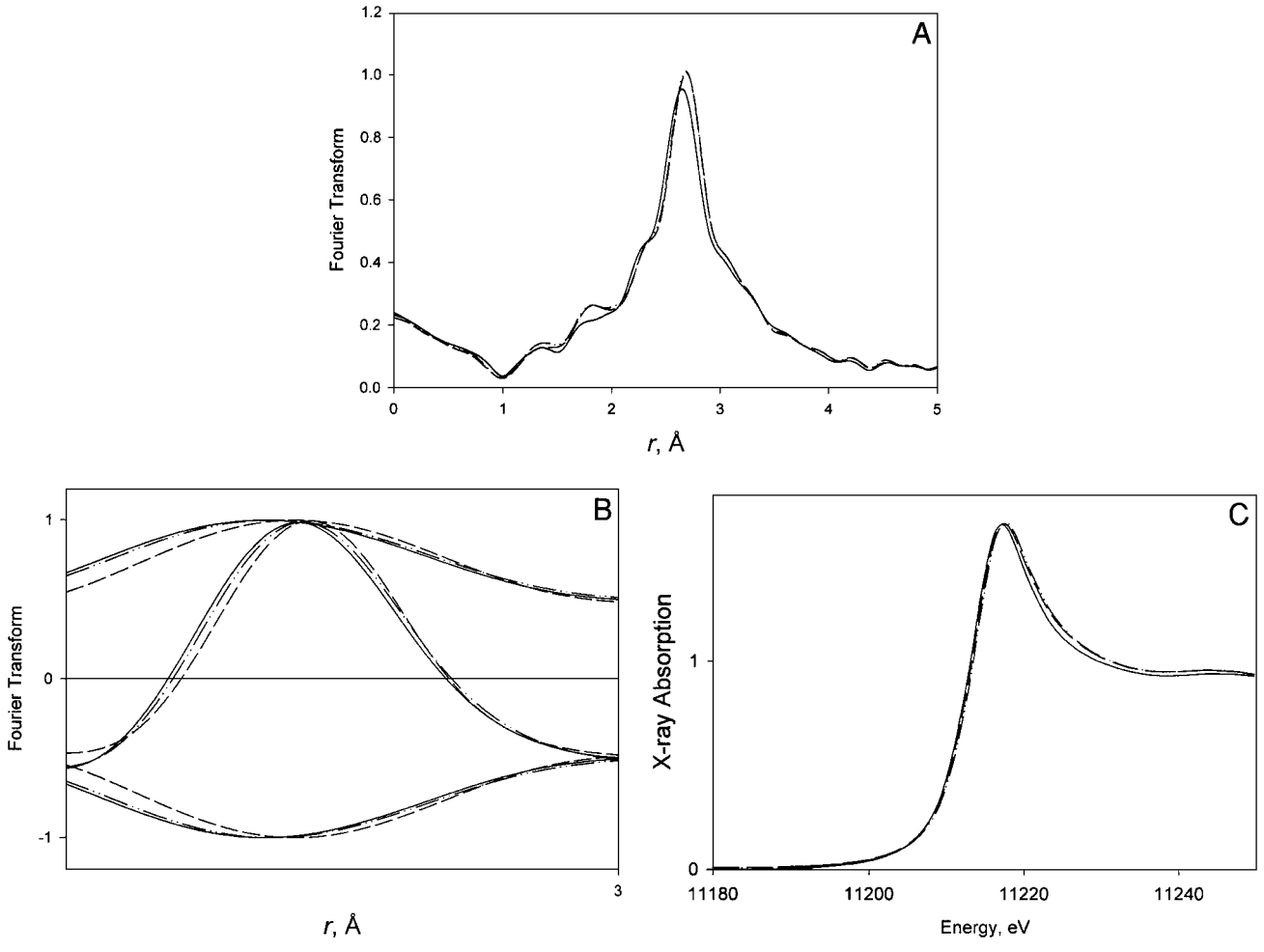

FIG. 6. Comparison of the X-ray absorption data characterizing supported iridium aggregates formed by treatment of $[Ir_6(CO)_{16}]$ supported in the uncalcined zeolite in H_2 at 300°C: (A) Magnitude of Fourier transform (k^0-weighted, Ir–Ir phase- and amplitude-corrected) of EXAFS data characterizing sample with gas flowing through the cell containing H_2 and propene in N_2 carrier gas with compositions of (0% H_2, 6% propene) (solid line), (2% H_2, 2% propene) (dotted-dashed line), and (6% H_2, 0% propene) (dashed line). (B) Scaled imaginary part and magnitude of Fourier transform (k^0-weighted, Ir–Ir phase- and amplitude-corrected) of EXAFS data characterizing sample with gas flowing through the cell containing H_2 and propene in N_2 carrier gas with compositions of (0% H_2, 6% propene) (solid line), (2% H_2, 2% propene) (dotted-dashed line), and (6% H_2, 0% propene) (dashed line). (C) XANES data characterizing sample with gas flowing through the cell containing H_2 and propene in N_2 carrier gas with compositions of (0% H_2, 6% propene) (solid line), (2% H_2, 2% propene) (dotted-dashed line), and (6% H_2, 0% propene) (dashed line).

and catalytic hydrogenation of propene occurring, the partially decarbonylated clusters and aggregates of iridium were characterized by Ir–Ir and Ir–low-Z contributions (Table 6). The data indicate no difference between the Ir–Ir first-shell coordination number and bonding distance characterizing the iridium clusters (or aggregates) catalyzing propene hydrogenation (Table 6; Figs. 5A and 5B and Figs. 6A and 6B) and those clusters (or aggregates) in H_2 only (Table 4). There was no observed effect of changes in the propene partial pressure on the Ir–Ir first-shell coordination number or bonding distance characterizing the iridium clusters as long as H_2 was present in the gas phase. These results indicate the lack of change in cluster or aggregate size or framework structure during catalysis.

X-Ray Absorption Near Edge Data

Near edge data are shown for supported rhodium (or iridium) clusters and aggregates in the presence of H_2, propene, or H_2/propene (Figs. 3C, 4C, 5C, and 6C); data are shown in Fig. 7 for the sample formed from NaY zeolite and $[Rh(CO)_2(acac)]$, for the NaY zeolite sample containing $[Rh_6(CO)_{16}]$, and for the sample formed by subsequent treatment of the former sample in H_2 at 200°C. Because the sample formed from the zeolite and $[Rh(CO)_2(acac)]$ had not been carbonylated or otherwise treated, the rhodium is inferred to have been in the initial +1 oxidation state. The XANES spectrum of the $[Rh(CO)_2(acac)]$-containing sample has only one broad peak, but the spectrum of the $[Rh_6(CO)_{16}]$-containing sample shows a sharp peak (or

TABLE 6

EXAFS Results Characterizing NaY Zeolite-Supported Rhodium and Iridium Clusters or Aggregates in the Presence of Propene + H_2[a]

Catalyst pretreatment conditions			Conditions during scan[d]				EXAFS parameters				Cluster or aggregate
Treatment gas/ Precursor	Temp (°C)	Support pretreatment[b,c]	% Propene	% H_2	Temp (°C)	Backscatterer[e,f]	N	R (Å)	$\Delta\sigma^2$ (Å^2)	ΔE_0 (eV)	
H_2/[$Rh_6(CO)_{16}$]	200	Yes	2	2	25	Rh	3.5	2.71	0.00357	−4.3	Cluster
						O	0.7	2.29	−0.00291	−20.0	
						C	3.6	2.02	0.01500	−14.4	
H_2/[$Rh_6(CO)_{16}$]	250	No	2	2	25	Rh	5.5	2.67	0.00345	5.5	Aggregate
						O	1.5	2.10	0.00384	−4.5	
						C	0.7	1.97	−0.00125	−14.6	
H_2/[$Ir_4(CO)_{12}$]	300	Yes	2.4	0.6	25	Ir	3.8	2.67	0.00515	3.6	Cluster
						O	1.3	2.26	0.00386	−9.1	
						C	3.2	2.00	0.01500	−14.5	
H_2/[$Ir_4(CO)_{12}$]	300	Yes	1.5	1.5	25	Ir	3.6	2.68	0.00506	2.8	Cluster
						O	1.4	2.25	0.00408	−9.9	
						C	3.3	1.99	0.01500	−14.7	
H_2/[$Ir_4(CO)_{12}$]	300	Yes	0.6	2.4	25	Ir	3.5	2.68	0.00368	−4.1	Cluster
						O	1.4	2.26	0.00363	−17.2	
						C	2.9	2.00	0.01255	−20.0	
H_2/[$Ir_6(CO)_{16}$]	300	Yes	2	2	25	Ir	4.7	2.69	0.00519	0.8	Aggregate
						O	1.1	2.22	0.00155	−3.1	
						C	3.2	1.98	0.01500	−7.4	

[a] Notation as in Table 2.
[b] If no, the support was evacuated at room temperature for 12 h (following gas treatment for samples treated in O_2).
[c] If yes, the support was calcined by flowing O_2 over the support at 300°C, followed by evacuation at 300°C for 12 h.
[d] When the sample was not under vacuum, the balance of the gas phase was N_2.
[e] For rhodium samples, an additional long Rh–O contribution was fitted (typical values: $N = 1.7$, $R = 3.0$ Å, $\Delta\sigma^2 = -0.004$ Å^2, $\Delta E_0 = -10$ eV).
[f] Additionally, a long Ir–O contribution (typical values: $N = 0.5$, $R = 2.8$ Å, $\Delta\sigma^2 = -0.003$ Å^2, $\Delta E_0 = -20$ eV) and an Ir–Al contribution (typical values: $N = 0.1$, $R = 1.5$ Å, $\Delta\sigma^2 = -0.002$ Å^2, $\Delta E_0 = 20$ eV) were fitted.

shoulder) with less intensity preceding a broader peak (or shoulder) at higher energy than the broad peak observed for the former sample (Fig. 7A). Partial decarbonylation of the [$Rh_6(CO)_{16}$]-containing sample in H_2 results in some filling in of the valley between the sharp and broad peaks, indicating a small increase in the oxidation state of the metal (Fig. 7B). Therefore, it is expected that the spectra of samples containing both reduced and cationic rhodium will

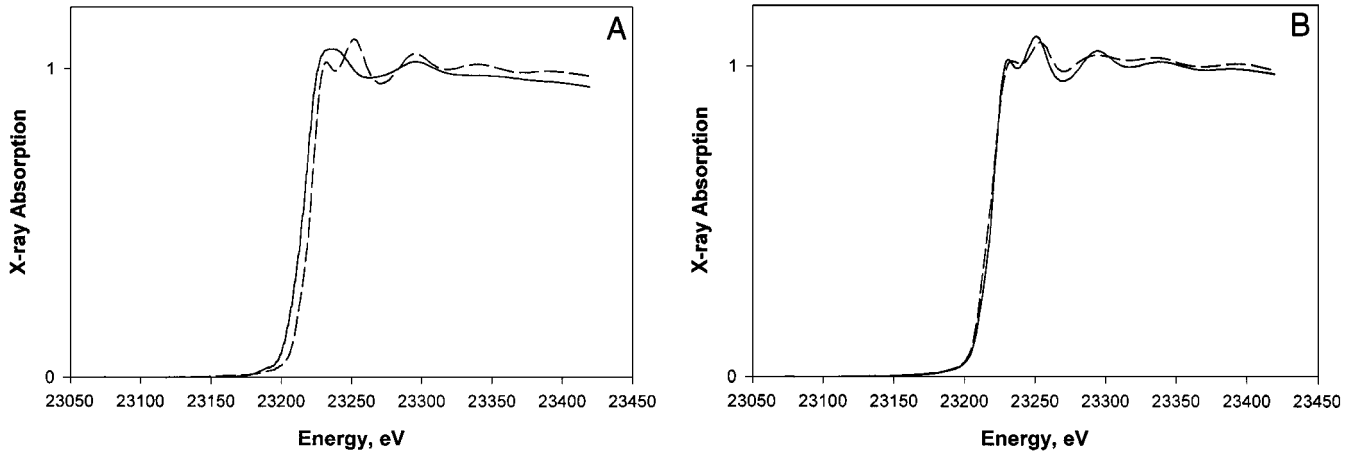

FIG. 7. (A) Comparison of the XANES data characterizing the sample formed from the zeolite and [$Rh(CO)_2$(acac)] (solid line) and NaY zeolite-supported [$Rh_6(CO)_{16}$] (dashed line). (B) Comparison of the XANES data characterizing NaY zeolite-supported [$Rh_6(CO)_{16}$] (solid line) and the sample formed by subsequent partial decarbonylation in H_2 at 200°C (dashed line).

TABLE 7

EXAFS Results Characterizing NaY Zeolite-Supported Rhodium Aggregates in the Presence of Propene + H_2[a]

Catalyst pretreatment conditions			Conditions during scan[d]				EXAFS parameters			
Treatment gas/ Precursor	Temp (°C)	Support pretreatment[b,c]	% Propene	% H_2	Temp (°C)	Backscatterer[e,f]	N	R (Å)	$\Delta\sigma^2$ (Å^2)	ΔE_0 (eV)
H_2/[$Rh_6(CO)_{16}$]	250	No	0	0	Liquid N_2	Rh	5.9	2.67	0.00264	6.1
						O	0.8	2.12	0.00367	−1.2
						C	1.0	1.87	0.00707	19.5
H_2/[$Rh_6(CO)_{16}$]	250	No	0	100	60	Rh	5.5	2.69	0.00309	3.8
						O	0.8	2.10	0.00616	4.4
						C	0.9	1.92	0.00268	0.2
H_2/[$Rh_6(CO)_{16}$]	250	No	10	90	60	Rh	5.9	2.69	0.00343	2.8
						O	0.6	2.13	0.00352	0.7
						C	0.7	1.95	0.00116	−3.6
H_2/[$Rh_6(CO)_{16}$]	250	No	10	90	100	Rh	6.2	2.69	0.00402	2.5
						O	0.5	2.10	−0.00190	−8.7
						C	0.6	1.97	−0.00331	−20.0
H_2/[$Rh_6(CO)_{16}$]	250	No	10	90	140	Rh	6.3	2.68	0.00473	3.1
						O	1.1	2.06	0.00282	10.4
						C	1.7	1.95	0.00467	−7.4

[a] Notation as in Table 2.
[b] If no, the support was evacuated at room temperature for 12 h (following gas treatment for samples treated in O_2).
[c] If yes, the support was calcined by flowing O_2 over the support at 300°C, followed by evacuation at 300°C for 12 h.
[d] When the sample was not under vacuum, the balance of the gas phase was N_2.
[e] For rhodium samples, an additional long Rh–O contribution was fitted (typical values: $N = 1.7$, $R = 3.0$ Å, $\Delta\sigma^2 = -0.004$ Å^2, $\Delta E_0 = -10$ eV).
[f] Additionally, a long Ir–O contribution (typical values: $N = 0.5$, $R = 2.8$ Å, $\Delta\sigma^2 = -0.003$ Å^2, $\Delta E_0 = -20$ eV) and an Ir–Al contribution (typical values: $N = 0.1$, $R = 1.5$ Å, $\Delta\sigma^2 = -0.002$ Å^2, $\Delta E_0 = 20$ eV) were fitted.

exhibit some filling in of the valley between the sharp and broad peak.

EXAFS Data Measured at Temperatures up to 140°C

Partially decarbonylated rhodium aggregates were characterized by *in situ* EXAFS spectroscopy at temperatures of 60, 100, or 140°C; the gas flowing through the cell contained 10% propene in H_2 (Table 7). The data were fitted satisfactorily by a Rh–Rh contribution and Rh–low-Z contributions (Table 7; Fig. 8). There was no detectable effect of temperature on the Rh–Rh first-shell coordination number or Rh–Rh distance, but the Debye–Waller factor increased with increasing temperature, as expected. The k-range used in the fitting and the standard deviations in the EXAFS function for each sample were typically 4.2–14.6 Å^{-1} and 0.002, respectively.

Effect of Contaminant Oxygen

Rhodium clusters were exposed to a gas mixture containing propene, H_2, and N_2, when the propene was fed without passing through the usual trap. The EXAFS data (not shown) include almost no oscillations for values of $k > 10$ Å^{-1}. Data analysis gave no evidence of a metal–metal contribution near 2.7 Å. These results indicate that the clusters had oxidatively fragmented.

Propene Hydrogenation Catalyzed by Zeolite-Supported Rhodium and Zeolite-Supported Iridium

Catalytic activity data characterizing rhodium or iridium clusters (or aggregates), obtained for the hydrogenation

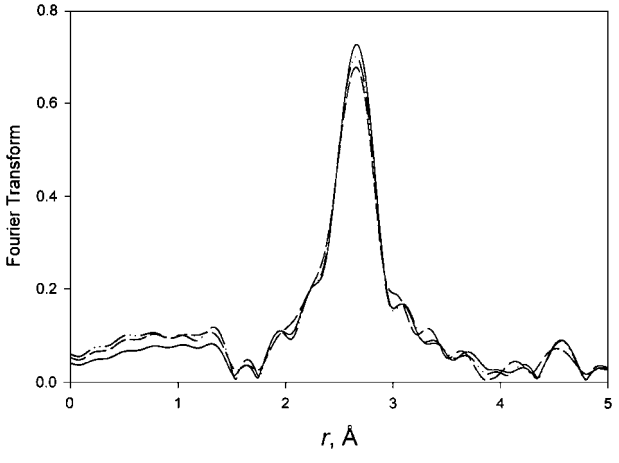

FIG. 8. Comparison of the X-ray absorption data characterizing supported rhodium aggregates formed by treatment of [$Rh_6(CO)_{16}$] in the calcined zeolite in H_2 at 250°C: Magnitude of Fourier transform (k^0-weighted, Rh–Rh phase- and amplitude-corrected) of EXAFS data characterizing sample with gas flowing through the cell containing 90% H_2 and 10% propene at temperatures of 60°C (solid line), 100°C (dotted-dashed line), and 140°C (dashed line).

TABLE 8

Catalysis of Toluene Hydrogenation by Rhodium or Iridium Clusters Formed from $[Rh_6(CO)_{16}]$ or $[Ir_4(CO)_{12}]$ in Calcined NaY Zeolite

				Propene : H_2 molar ratio[a]		
	Catalyst pretreatment			0.29	1.08	4.13
Precursor	Gas	Temp (°C)	Time (h)	Conversion of propene	Conversion of propene	Conversion of propene
$[Rh_6(CO)_{16}]$	H_2	200	2	0.29	0.24	0.16
$[Ir_4(CO)_{12}]$	H_2	300	2	0.19	0.14	0.05

[a] Total flow rate of gas was 100 ml(NTP)/min. Gas was 3% (H_2 + propene) in a balance of N_2.

of propene at 25°C taking place in the EXAFS cell, are summarized in Table 8. The propene conversions in the presence of rhodium ranged from 16 to 29%; conversions in the presence of iridium ranged from 5 to 19%. Steady-state operation was observed after 2 h on stream. Conversion in the absence of catalyst was negligible.

DISCUSSION

Effect of Adsorbates on the Structures of Supported Metal Clusters and Aggregates

Structures of supported metal clusters and aggregates in the presence of H_2 or propene. The data show that the metal frameworks of the clusters and aggregates remained intact in the presence of H_2 or propene, but metal–metal distances may have changed by about 0.04 and 0.03 Å upon adsorption of propene rather than hydrogen. As these values are close to the expected uncertainty in bonding distance (about 0.03 Å), it might be argued that the changes are not significant. However, we do no rule out the possibility that they are significant, because the shifts observed in the positions of the imaginary parts of the Fourier transforms characterizing the clusters in the presence of H_2 and of propene (Figs. 3B, 4B, 5B, and 6B), which roughly indicate bonding distances, without exception indicate the stated changes in the metal–metal bonding distances and because the differences in Rh–Rh and Ir–Ir bonding distances are similar to those seen in the results of Gallezot (42, 43), whose measurements of radial electron distributions showed that the Pt–Pt bonding distance in platinum aggregates in zeolite Y decreased from 2.77 Å with hydrogen adsorbed to 2.71 Å with benzene adsorbed. Chemisorption of hydrogen decreases the electron density between metal atoms and allows metal–metal bonds to relax (44).

Evidence of propene adsorption. The metal–low-Z scatterer contributions do not provide accurate enough data to identify adsorbates on the clusters or aggregates, but the near-edge data give evidence suggesting adsorption of propene on rhodium. The Rh K-edge XANES regions characterizing both rhodium clusters and aggregates show small changes in the absorption edge upon addition of propene to the EXAFS cell in the absence of H_2 (Figs. 3C and 4C). The changes observed (increased absorption at energies higher than those of the sharp peak or shoulder) for both clusters and aggregates suggest that adsorbed propene withdraws electron density from the rhodium.

Structures of supported clusters and aggregates during catalysis. The EXAFS data characterizing the rhodium and iridium clusters and aggregates during catalysis showed no changes in the metal framework structures. Thus, the data confirm the unsurprising conclusion that the supported metal aggregates are catalytically active species, and they also lead to the inference that the supported clusters of each metal themselves are also catalytically active. The near-edge data indicate that when H_2 was present in the gas phase, regardless of the presence of propene or of the cluster or aggregate size, the spectrum of the working catalyst was nearly the same as that of the same catalyst with only H_2 present (Figs. 3C, 4C, 5C, 6C). These results, combined with the EXAFS data indicating that the metal–metal distances in the working catalysts almost exactly match those of the same catalysts in the presence of H_2 while not matching those in the presence of propene, suggest that hydrogen was the predominantly adsorbed species during catalysis.

The data confirm the assumption made earlier that the clusters are catalytically active species and support the discussion of the effects of cluster size and support on catalytic performance presented elsewhere (45 and references cited therein).

Catalysis of Propene Hydrogenation by Supported Clusters and Aggregates

When mixtures of propene and H_2 in N_2 similar to that used in the EXAFS experiments flowed through the EXAFS cell, they were catalytically converted into propane, with a typical conversion being about 20% under conditions matching those of the EXAFS experiments (Table 8). These results confirm the implicit assumption above that the EXAFS data recorded with the propene/H_2 mixture

characterize catalysts in the working state. The data show that most of the gas in the cell was propene + H_2 (in N_2) rather than product propane.

As the conversions were relatively low, the composition of the gas phase did not depend significantly on the position within the cell. Furthermore, estimates of mass transfer resistance within the catalyst wafer indicate that there were no large concentration gradients (46). These results show that the composition of the entering gas phase roughly represented that throughout the catalyst in the cell, and, thus, we infer that the EXAFS data provide information about the structure of the sites responsible for catalysis in a nearly uniform environment. The catalysis data support the inferences drawn above about the catalytically active species.

Strengths and Limitations of EXAFS Data Characterizing Working Catalysts

The EXAFS data provide good evidence of the metal framework structures, even at temperatures as high as 140°C; this information demonstrates the stability of the supported clusters and aggregates under catalytic reaction conditions. The data characterizing the low-Z scatterers are, however, of relatively low quality and not sufficient for identification of adsorbed species. Even with the smallest and most nearly uniform clusters, it does not seem to be feasible to determine structures of adsorbed species with the EXAFS technique as we have used it.

The EXAFS data obtained at the higher temperatures (up to 140°C, Table 7) show that rhodium aggregates were stable under these conditions. However, the amplitude of the EXAFS oscillations and the signal to noise ratio were quite low at the highest temperature, corresponding to the increasing Debye–Waller factors with increasing temperatures (Table 7); these changes are expected, indicating the increased disorder at higher temperatures.

Because the quality of the data characterizing the metal framework structures is greatest at the lowest temperatures, *in situ* EXAFS spectroscopy is expected to be of most value for highly active catalysts, which can be investigated in the working state at low temperatures.

CONCLUSIONS

The EXAFS data show that the zeolite-supported metal clusters and aggregates (rhodium or iridium) were stable at room temperature in the presence of H_2, of propene, and of propene/H_2 with catalytic hydrogenation occurring. These supported clusters, like the aggregates, are inferred to be catalytically active for propene hydrogenation. Rhodium aggregates retain their metal frameworks during catalysis at temperatures as high as 140°C. The EXAFS data indicate a lack of changes in metal framework structures under the observed conditions (except when O_2 contaminant was present), but they are not sufficient to provide evidence of adsorbate structures. The EXAFS data seem to indicate shorter metal–metal distances with propene in contact with the metal surfaces, but this suggestion is in doubt because the apparent changes in distance are nearly the same as the experimental uncertainty.

ACKNOWLEDGMENTS

The research was supported by the National Science Foundation (Grant CTS-9617257). We acknowledge the support of the U.S. Department of Energy, Division of Materials Sciences, under Contract DE-FG05-89ER45384, for its role in the operation and development of beam line X-11A at the National Synchrotron Light Source (NSLS). The NSLS is supported by the Department of Energy, Division of Materials Sciences and Division of Chemical Sciences, under Contract DE-AC02-76CH00016. We thank the staff of beam line X-11A for their assistance. The X-ray absorption data were analyzed with the XDAP software (47).

REFERENCES

1. McIntyre, B. J., Salmeron, M., and Somorjai, G. A., *J. Catal.* **164**, 184 (1996).
2. Yoon, H. A., Salmeron, M., and Somorjai, G. A., *Surf. Sci.* **373**, 300 (1997).
3. Crew, W. W., and Madix, R. J., *Surf. Sci.* **356**, 1 (1996).
4. Crew, W. W., and Madix, R. J., *Surf. Sci.* **349**, 275 (1996).
5. Zambelli, T., Wintterlin, J., and Ertl, G., *Science* **273**, 1688 (1996).
6. Frahm, R., Clausen, B. S., Molenbroek, A. M., and Steffensen, G., *in* "Proceedings of the 9th International Conference on X-Ray Absorption Fine Structure," Abstract 630. Grenoble, France, 1996.
7. Thomas, J. M., and Greaves, G. N., *Science* **265**, 1675 (1994).
8. Maschmeyer, T., Sprunger, T., Ruan, L., Olesen, L., Stensgaard, I., and Lægsgaard, E., *Top. Catal.* **1**, 325 (1994).
9. Muetterties, E. L., Rhodin, T. N., Band, E., Brucker, C. F., and Pretzer, W. R., *Chem. Rev.* **79**, 91 (1979).
10. Ertl, G., *in* "Metal Clusters in Catalysis" (B. C. Gates, L. Guczi, and H. Knözinger, Eds.), p. 577. Elsevier, Amsterdam, 1986.
11. van Zon, F. B. M., Maloney, S. D., Gates, B. C., and Koningsberger, D. C., *J. Am. Chem. Soc.* **115**, 10317 (1993).
12. Maloney, S. D., Kelley, M. J., Koningsberger, D. C., and Gates, B. C., *J. Phys. Chem.* **95**, 9406 (1991).
13. Kawi, S., Chang, J.-R., and Gates, B. C., *J. Phys. Chem.* **97**, 5375 (1993).
14. Zhao, A., and Gates, B. C., *J. Am. Chem. Soc.* **118**, 2458 (1996).
15. Kawi, S., Chang, J.-R., and Gates, B. C., *J. Phys. Chem.* **97**, 10599 (1993).
16. Kawi, S., Chang, J.-R., and Gates, B. C., *J. Am. Chem. Soc.* **115**, 4830 (1993).
17. Weber, W. A., and Gates, B. C., *J. Phys. Chem. B* **101**, 10423 (1997).
18. Weber, W. A., Phillips, B. L., and Gates, B. C., to be published.
19. Jentoft, R. E., Deutsch, S. E., and Gates, B. C., *Rev. Sci. Instrum.* **67**, 2111 (1996).
20. Wyckoff, R. W. G., *in* "Crystal Structures," 2nd ed., Vol. 1, p. 10. Wiley, New York, 1963.
21. Rehr, J. J., Mustre de Leon, J., Zabinsky, S. I., and Albers, R. C., *J. Am. Chem. Soc.* **113**, 5135 (1991).
22. Coey, J. M. D., *Acta. Crystallogr.* **B26**, 1876 (1970).
23. Mason, R., and Rae, A. I. M., *J. Chem. Soc. (A)* 778 (1968).
24. Trömel, M., and Lupprich, E. Z., *Anorg. Chem.* **414**, 160 (1975).
25. Churchill, M. R., and Hutchinson, J. P., *Inorg. Chem.* **17**, 3528 (1978).
26. van Zon, F. B. M., Maloney, S. D., Gates, B. C., and Koningsberger, D. C., *J. Am. Chem. Soc.* **115**, 10317 (1993).
27. van Zon, J. B. A. D., Ph.D. dissertation, Eindhoven Univ. of Technology, The Netherlands, 1988.

28. Kirlin, P. S., van Zon, F. B. M., Koningsberger, D. C., and Gates, B. C., *J. Phys. Chem*. **94**, 8439 (1990).
29. van Zon, J. B. A. D., Koningsberger, D. C., van't Blik, H. F. J., and Sayers, D. E., *J. Chem. Phys.* **82**, 5742 (1985).
30. Koningsberger, D. C., and Prins, R. (Eds.) "X-Ray Absorption: Principles, Applications, Techniques of EXAFS, SEXAFS, and XANES." Wiley, New York, 1988.
31. Shannon, R. D., Vedrine, J. C., Naccache, and C., Lefebvre, F., *J. Catal.* **88**, 431 (1984).
32. Hanson, B. E., Davis, M. E., Taylor, D., and Rode, E., *Inorg. Chem*. **23**, 52 (1984).
33. Lefebvre, F., and Ben Taarit, Y., *Nouv. J. Chim*. **8**, 387 (1984).
34. Wong, T. T., Zhang, Z., and Sachtler, W. M. H., *Catal. Lett.* **4**, 365 (1990).
35. Rao, L.-F., Fukuoka, A., Kosugi, N., Kuroda, H., and Ichikawa, M., *J. Phys. Chem*. **94**, 5317 (1990).
36. Mantovani, E., Palladino, and N., Zanobi, A., *J. Mol. Catal.* **3**, 285 (1977/8).
37. Rode, E. J., Davis, M. E., and Hanson, B. E., *J. Catal.* **96**, 574 (1985).
38. Shriver, D. F., *J. Organomet. Chem*. **94**, 259 (1975).
39. Horwitz, C. P., and Shriver, D. F., *Adv. Organomet. Chem*. **23**, 219 (1984).
40. Garlaschelli, L., Martinengo, S., Bellon, P. L., Demartin, F., Manassero, M., Chiang, M. Y., Wei, C.-Y., and Bau, R., *J. Am. Chem. Soc.* **106**, 6664 (1984).
41. Kip, B. J., Duivenvoorden, F. B. M., Koningsberger, and D. C., Prins, R., *J. Catal.* **105**, 26 (1987).
42. Gallezot, P., and Bergeret, G., *J. Catal.* **72**, 294 (1981).
43. Gallezot, P., *J. Chim. Phys.* **78**, 381 (1981).
44. Vaarkamp, M., Mojet, B. L., Kappers, M. J., Miller, J. T., and Koningsberger, D. C., *J. Phys. Chem*. **99**, 16067 (1995).
45. Weber, W. A., and Gates, B. C., *J. Catal.*, in press.
46. Weber, W. A., Ph.D. dissertation, Univ. of California, Davis, 1998.
47. Vaarkamp, M., Linders, J. C., and Koningsberger, D. C., *Physica B* **209**, 159 (1995).